Supplementary Material: Excitonic Mott insulator in a Bose-Fermi-Hubbard system of moiré WS_2/WSe_2 heterobilayer

Beini Gao,[1,*] Daniel G. Suárez-Forero*,[1,†] Supratik Sarkar,[1,*] Tsung-Sheng Huang,[1] Deric Session,[1] Mahmoud Jalali Mehrabad,[1] Ruihao Ni,[2] Ming Xie,[3] Jonathan Vannucci,[1] Sunil Mittal,[1] Kenji Watanabe,[4] Takashi Taniguchi,[4] Atac Imamoglu,[5] You Zhou,[2,6] and Mohammad Hafezi[1,7,‡]

[1] *Joint Quantum Institute (JQI), University of Maryland, College Park, MD 20742, USA*
[2] *Department of Materials Science and Engineering, University of Maryland, College Park, MD 20742, USA*
[3] *Condensed Matter Theory Center, University of Maryland, College Park, MD 20742, USA*
[4] *National Institute for Materials Science, Tsukuba, Japan*
[5] *Institute of Quantum Electronics, ETH Zurich, CH-8093 Zurich, Switzerland*
[6] *Maryland Quantum Materials Center, College Park, Maryland 20742, USA*
[7] *Institute for Theoretical Physics, ETH Zurich, 8093 Zurich, Switzerland*

Device fabrication

The WSe_2/WS_2 heterostructure shown in Fig. S1 was fabricated using a dry-transfer method with a stamp made of a poly(bisphenol A carbonate) (PC) layer on polydimethylsiloxane (PDMS) [1]. All flakes were exfoliated from bulk crystals onto Si/SiO_2 (285 nm) and identified by their optical contrast. The top/bottom gates and TMD contact are made of few-layer graphene. The PC stamp and samples were heated to 60°C during the pick-up steps and released from the stamp to the substrate at 180°C. The PC residue on the device was removed in chloroform followed by a rinse in isopropyl alcohol and ozone clean. Sample transfer was performed in an argon-filled glovebox for improved interface quality. The electrodes consist of 3.5 nm of chromium and 70 nm of gold. They were fabricated using standard electron-beam lithography techniques and thermal evaporation.

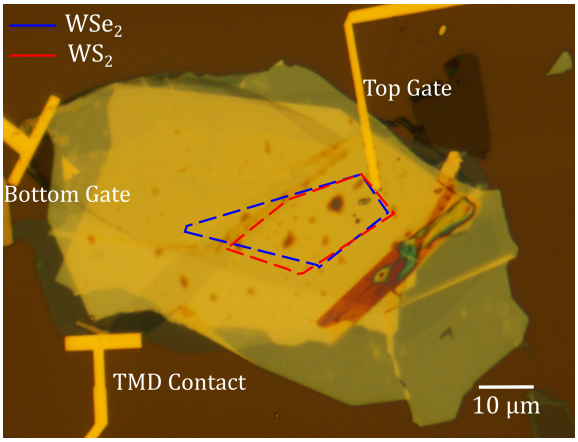

FIG. S1: Microscope image of the WS_2/WSe_2 heterostructure device.

Optical measurements

The sample is kept in a dilution refrigerator at a temperature of 3.5K. For photoluminescence measurements, we use a confocal microscopy setup with an objective of magnification 70× and numerical aperture NA = 0.82. Our pumping source is a pulsed Ti:Sapphire laser tuned at 720nm (1.722eV), with a pulse duration of 100fs and a repetition rate of ∼ 80 MHz. A half-waveplate placed before a polarizing beam-splitter is rotated to control the pump power. Additionally, an optical chopper system at 800Hz is used to prevent sample heating while having a high pump intensity. A 750nm long-pass filter was used to block the residual pump laser before collecting the PL emission in a spectrometer equipped with a 300 grooves per mm diffraction grating and a CCD camera. The schematic of the setup is shown in Fig. S2.

For the diffusion measurements, we used a continuous-wave (CW) Ti:Sapphire laser tuned at 708nm. The rest of the optical measurement setup was similar. By applying a spatial filter to the reconstructed image of the diffusion pattern, we obtain spectral and spatial data of the exciton emission. This allows us to image the spatial diffusion of each spectral component and extract the diffusion length.

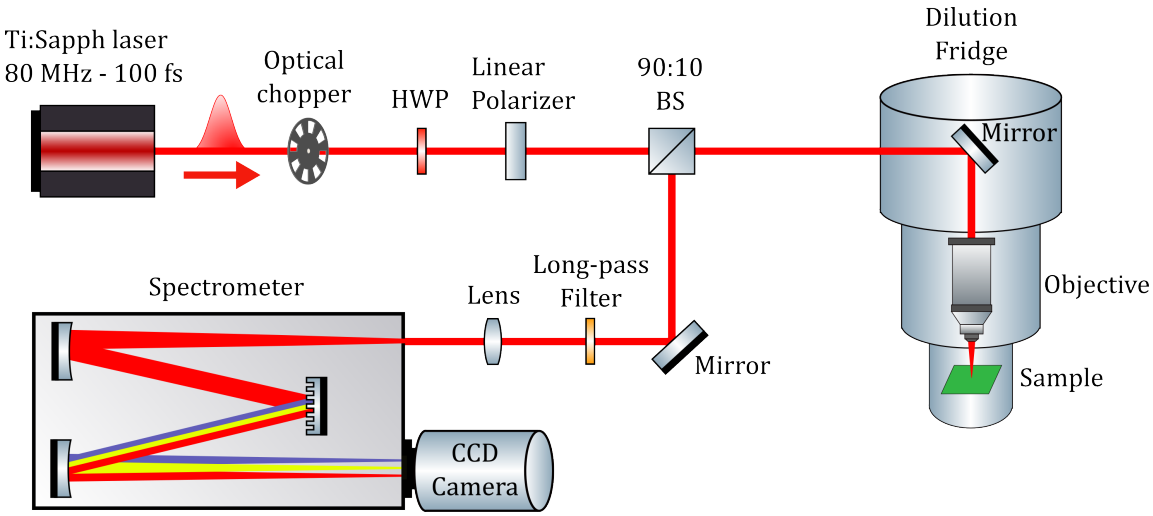

FIG. S2: Schematic of the experimental setup. HWP=Half-wave plate, BS=Beam splitter

Electronic filling factor calibration

The electronic filling factor (ν_e) can be estimated by combining the information about the crystalline structure of the bilayer device and a parallel capacitor model, as follows:

Determination of moiré density n_0: In a purely fermionic Mott insulating state, the heterostructure will host one electron per moiré unit cell. The charge density in this case is given by n_0, and it can be directly determined by the moiré periodicity through the relationship $n_0 = 1/({L_M}^2 \sin \pi/3)$. Here, $L_M = a/\sqrt{\delta^2 + \theta^2}$ is the size of the moiré superlattice, $\delta = (a - a')/a \approx 4\%$ is

the lattice mismatch between WSe_2 ($a = 0.328$nm) and WS_2 ($a' = 0.315$nm), and θ is the twist angle between the two layers. Assuming $0° \leq \theta \leq 1°$, we obtain $1.72 \times 10^{12}\text{cm}^{-2} \leq n_0 \leq 2.04 \times 10^{12}\text{cm}^{-2}$.

Determination of electron density n_e: From a parallel capacitor model, we can deduce the expression for the electron density (n_e) in the bilayer. For a dual gate device, n_e is given by:

$$n_e = \frac{\epsilon_r \epsilon_0 \Delta V_g}{d_t} + \frac{\epsilon_r \epsilon_0 \Delta V_g}{d_b},$$

where V_g is the symmetrically applied gate voltage and $d_t \approx d_b \approx 40$nm are the thicknesses of the top and bottom hBN dielectrics, respectively. They are determined from the optical contrast of the hBN flakes under the microscope. ϵ_0 is the vacuum permittivity, and $\epsilon_r \approx 3$ is the relative permittivity of hBN [2]. Having the moiré density n_0 and the electron density n_e, the electronic (fermionic) filling factor can be expressed as $\nu_e = n_e/n_0$. From this model we deduce that the gate voltage at which the electronic Mott insulator is established lies in the range $2.65\text{ V} < V_g < 3.04\text{ V}$. Where we are taking into account that the neutral region extends up to $V_g = 0.58$ V. This estimation is in good agreement with our experimental data for reflectivity and PL. The results, displayed in Fig. S3 show a consistent change in the optical response of the device at $V_g = 2.98$ V. For the reflectivity (panel a), we observe a shift in the intralayer exciton energy. For the PL (panel b), a corresponding energy transition is observed for the interlayer exciton.

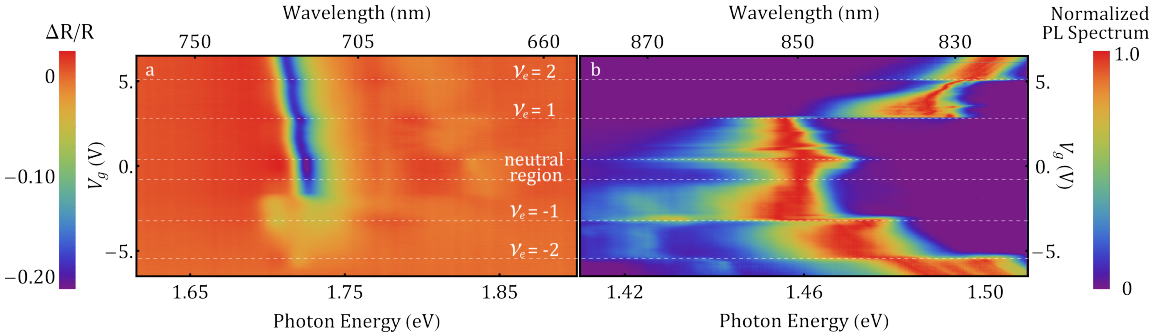

FIG. S3: Reflection and photoluminescence spectra of our WS_2/WSe_2 heterobilayer device.

Total emitted PL vs. Pump Intensity

Due to the saturability of real semiconductor materials upon an intense optical pump, the laser intensity I is not a suitable parameter to estimate the total exciton density in the bilayer. One can corroborate this from Fig. S4, by noticing that the emitted PL power does not follow a linear trend with increasing I. A more suitable quantity to monitor the changes in the excitonic density is the total emitted PL power. This quantity can be considered proportional to the total number of excitons formed in the structure, with the proviso that the radiative decay of the excitons does not change considerably within the phase space determined by V_g and I. For this reason, figures 2 and 3 of the main text display the total PL power instead of the pump intensity. For simplicity, all the PL powers presented in the main text are normalized to a factor 10^6.

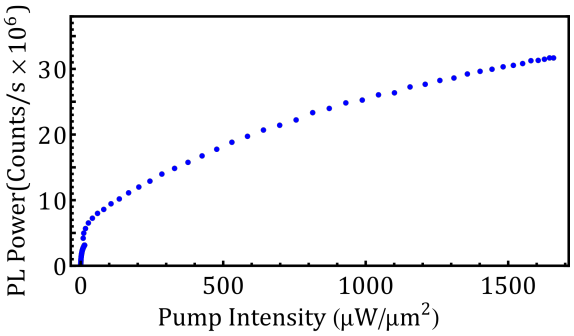

FIG. S4: Pump intensity dependent total PL power at $V_g = 0$V

Data analysis

To obtain relevant information about the collected spectra, we use a fitting routine. This procedure allows us to obtain the PL emission central energy, linewidth, and integrated PL power of each exciton line (X_1 and X_2). First, the PL spectra are processed by removing background noise and applying a low-pass Butterworth filter. After that, we extract the peaks from each spectrum by imposing constraints on the energy range, linewidth, prominence, and relative amplitude to the noise level. By setting a tolerance to the numerical error of the obtained values of intensity and energy of each peak, we fit each spectrum to a multi-Lorentzian distribution. From the fitting functions, we extract the central energies of X_1 and X_2 and integrate them over the obtained distributions to get the individual PL power.

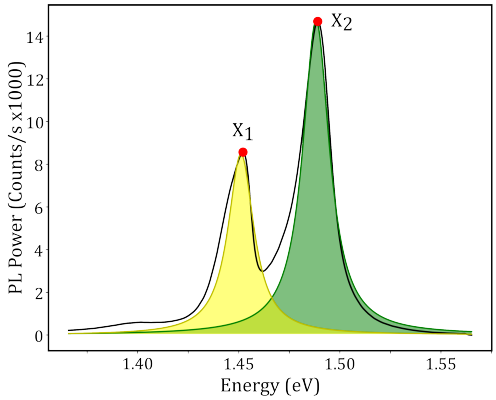

FIG. S5: A typical PL spectrum ($V_g = 2.1$ V and $I = 2226$ μW/μm^2) with the fitting functions obtained from the numerical method.

Modeling X_1 and X_2

To obtain further insights into the physical mechanism dominating the system dynamics, we make a theoretical analysis using a 2-band model, as mentioned in the main text. Our goal is to deduce an analytical expression for the observed saturation behavior of the PL power from the X_1 population. This is achieved by considering the steady state of the system in a continuous-wave excitation regime. A population of electron-hole pairs n_{eh} is created by a Rabi-driving $\Omega(t)$. The charged plasma cascades down and relaxes to create n_1 singly occupied moiré sites (X_1) and n_2 doubly occupied sites (X_2). The formation of those states depends on the relaxation rate of the plasma (Γ_{relax}), the maximum number of available lattice sites ($n_{\mathrm{max}}(\nu_{\mathrm{e}})$), and a β factor, which determines the probability of the plasma to decay into the X_1 state. Under these conditions, the system's dynamics can be described by the set of equations:

$$\frac{\mathrm{d}n_{\mathrm{eh}}}{\mathrm{d}t} = \eta\left|\Omega(t)\right|^2 - \Gamma_{\mathrm{relax}} n_{\mathrm{eh}} \tag{1a}$$

$$\frac{\mathrm{d}n_1}{\mathrm{d}t} = \Gamma_{\mathrm{relax}}\beta\frac{n_{\mathrm{max}}(\nu_e) - n_1}{n_{\mathrm{max}}(\nu_e)} n_{\mathrm{eh}} - \Gamma_1 n_1 \tag{1b}$$

$$\frac{\mathrm{d}n_2}{\mathrm{d}t} = \Gamma_{\mathrm{relax}}\left(1 - \beta\frac{n_{\mathrm{max}}(\nu_e) - n_1}{n_{\mathrm{max}}(\nu_e)}\right) n_{\mathrm{eh}} - \Gamma_2 n_2 \tag{1c}$$

where η is the efficiency of the optical generation of electron-hole pairs and Γ_1 (Γ_2) is the decay rate of the excitonic states in a singly (doubly) occupied site. In a steady state condition, from Eq. 1b, we can obtain an analytical expression for n_1:

$$n_1 = \frac{\Gamma_{\mathrm{relax}}\beta n_{\mathrm{eh}}}{\Gamma_1 + \Gamma_{\mathrm{relax}}\beta\frac{n_{\mathrm{eh}}}{n_{\mathrm{max}}}} \tag{2}$$

In this regime n_{eh} reaches an asymptotic value $n_{\mathrm{eh}} = \frac{\eta}{\Gamma_{\mathrm{relax}}}\left|\Omega\right|^2$. To associate this expression with our experimental data, we take into account that $n_{\mathrm{eh}}\Gamma_{\mathrm{relax}}$ is proportional to the total PL power and n_1 is proportional to the PL power (P_1) from the X_1 exciton band. After substituting variables we can conclude that the saturation behavior of X_1 should follow the functional form:

$$P_1 = \mathrm{P}_1^{\mathrm{max}}\frac{\mathrm{P}}{\mathrm{P} + \mathrm{P}_{\mathrm{sat}}} \tag{3}$$

where $P_1^{\mathrm{max}} = n_{\mathrm{max}}$ is proportional to the PL power from X_1 in an ideal Mott insulating state and $P_{\mathrm{sat}} = \Gamma_1 n_{\mathrm{max}}/\beta$ determines the total PL emission at which X_1 saturates. This expression is used as a fitting model for the PL power from the X_1 states upon increasing total PL power, and provides a mathematical tool to estimate the bosonic occupation of the moiré lattice. From this theoretical treatment, one can notice that the bosonic Mott insulating states are reached asymptotically. This means that P_1 can be arbitrarily close to P_1^{max} upon a high enough total PL power. In other words, the line that determines the Mott insulating phases in Figs. 1c, 2d and 3d is mathematically not achievable. For this reason, the intensity denoted as I^* in the referred figures, indicates the required pump intensity to drive the system into a state with a total population arbitrarily close to the lattice complete saturation.

Diffusion measurements

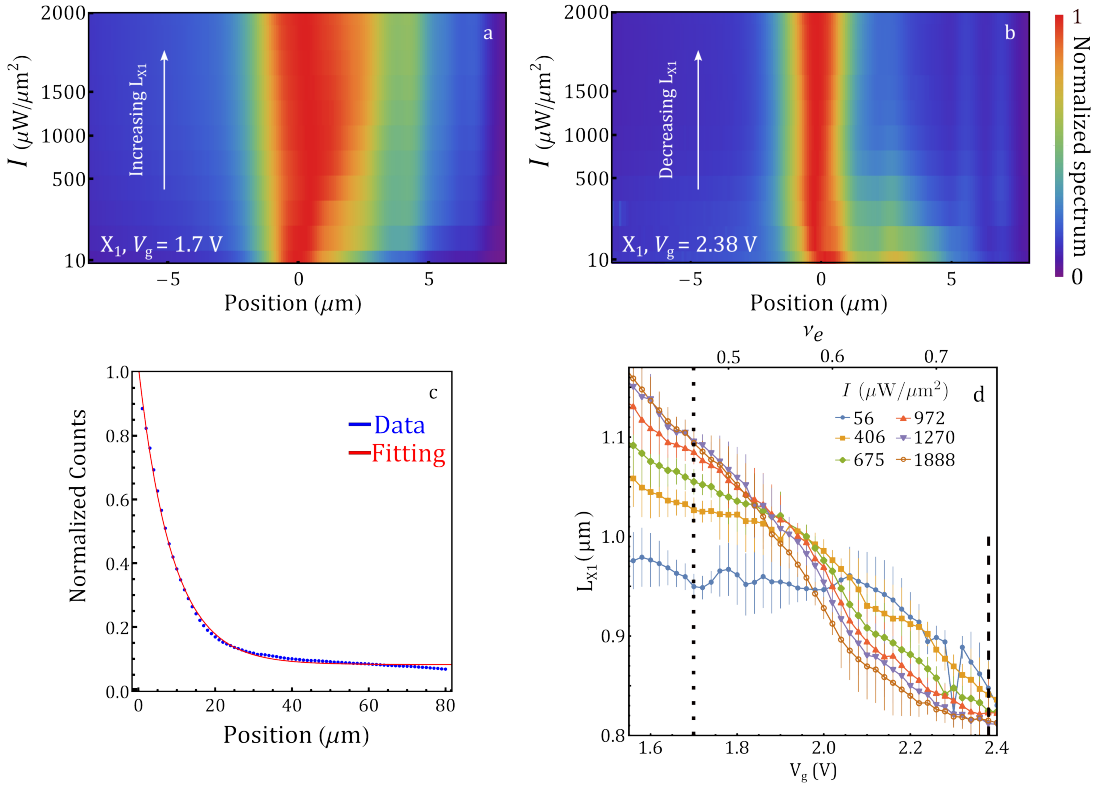

FIG. S6: (a-b) Pump intensity dependence of the X_1 spatial diffusion for $\nu_e \sim 0.47$ ($V_g = 1.7V$) (a) and $\nu_e \sim 0.75$ ($V_g = 2.38V$) (b). The panels show the inversion of the intensity dependence: from a diluted gas of bosons in panel a to a bosonic Mott insulator in panel b. (c) Exponential decay fitting of a typical X_1 diffusion pattern. (d) L_{X1} for a reduced range of V_g to highlight the power dependence inversion.

For the diffusion measurements, we use a continuous-wave laser tuned at 708 nm to create a steady population of excitons. By imaging the diffusion pattern with spectral resolution, we are capable of monitoring the diffusion properties of the X_1 and X_2 populations. We study the dependence of the diffusion length for each population as a function of V_g and I. To improve the spatial resolution, the image of the diffusion pattern is magnified 200 times. We spectrally resolve the signals emitted from X_1 and X_2. Next, we fit each spatial diffusion profile to a function of the form $A\exp(-x/L_{X_i}) + b$, where A is the PL power under the pumping laser spot, x is the propagation distance, L_{X_i} is the diffusion length of X_i and b is an offset that accounts for the base noise level. Fig. S6 (a-b) shows the obtained power dependence for L_{X_1} at $V_g = 1.7$ V and $V_g = 2.38$ V. We observe that L_{X_1} increases with pump power at 1.7 V but decreases at 2.38 V. This inversion in the power dependence accounts for the formation of incompressible excitonic states. It is worth mentioning that the scale of the I

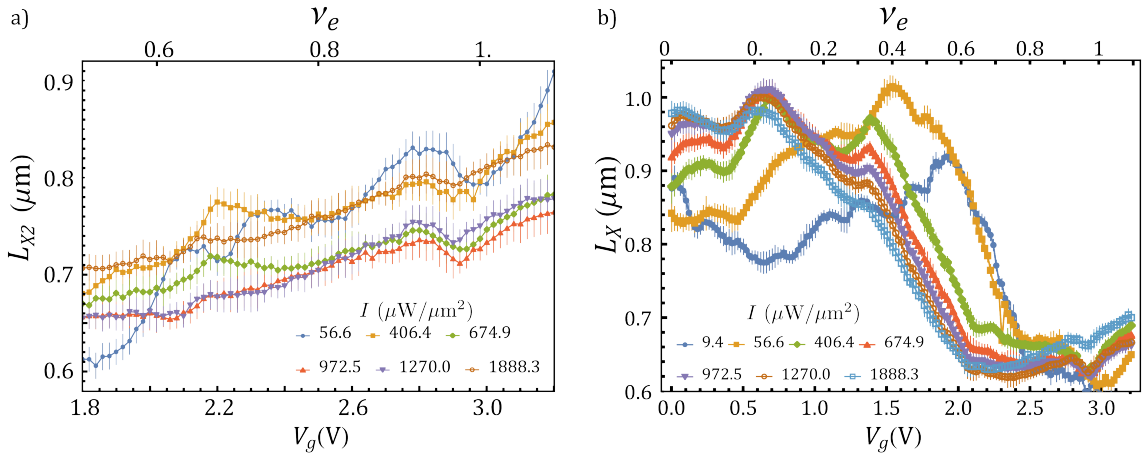

FIG. S7: (a)L_{X2} as a function of the gate voltage for a range of ν_e and for different I (b) L_X as a function of the gate voltage for a range of ν_e and for different I

axis is not linear, because the power was modified by changing the polarization of the pump laser with a half-wave plate. Panel c shows the fitting subroutine used to extract the diffusion length of X_1. Panel d shows the measured value of L_{X_1} for a range of V_g to highlight the inversion of the intensity dependence. The same analysis was performed for the diffusion of the X_2 states. The data (Fig. S7a) shows a shorter diffusion length, which makes it cumbersome to detect changes in L_{X2} due to the diffraction limit. However, in contrast to L_{X1}, the L_{X2} increases with increasing V_g, except for the reduction at $\nu_e \sim 1$, which can be attributed to the behavior of a population of excitons in presence of a fermionic Mott insulating state. We finally analyze the diffusion data with no spectral resolution. For $\nu_e < 1$, one can observe that the suppression of the diffusion takes place for lower V_g upon increasing pump intensity; a consequence of the bosonic saturation of the lattice due to the optical pump.

* These authors contributed equally to this work
† dsuarezf@umd.edu
‡ hafezi@umd.edu

[1] P. J. Zomer, M. H. D. Guimarães, J. C. Brant, N. Tombros, and B. J. van Wees, Applied Physics Letters **105**, 013101 (2014).
[2] H. C. P. Movva, B. Fallahazad, K. Kim, S. Larentis, T. Taniguchi, K. Watanabe, S. K. Banerjee, and E. Tutuc, Phys. Rev. Lett. **118**, 247701 (2017).